3D Computation of the Overhead Power Lines Electric Field

Tonći Modrić*, **Slavko Vujević, and Ivan Paladin**

Abstract—In this paper, a 3D quasistatic numerical algorithm for computation of the electric field produced by overhead power lines is presented. The real catenary form of the overhead power line phase conductors and shield wires is taken into account with an arbitrary number of straight thin-wire cylindrical segments of active and passive conductors. In order to obtain more precise results of the charge density distribution, segmentation is conducted for each overhead power line span separately. Moreover, the presence of the towers which distort the electric field and significantly reduce its magnitude is taken into account. Therefore, the towers of overhead power lines are approximated using thin-wire cylindrical segments of passive conductors with electric potential equal to zero. From self and mutual coefficients of these components, system of linear equations for computation of the charge density distribution was obtained. In the numerical example, electric field intensity distribution in the vicinity of towers and under the midspan of overhead power lines is shown. In order to verify the accuracy of the presented model, the obtained results are compared with similar published examples and results available in the literature.

1. INTRODUCTION

Extremely low-frequency (ELF) electric and magnetic fields caused by large time-harmonic currents and charges from the high-voltage substations and overhead power lines have been a subject of great interest due to possible adverse health effects [1–7]. The International Commission on Non-Ionizing Radiation Protection (ICNIRP) has assessed the available knowledge and published in 2010 guidelines for limiting exposure to time-varying electric and magnetic fields [8]. According to these guidelines, reference levels for 50 Hz electric field intensity are 10 kV/m for occupational exposure and 5 kV/m for general public exposure.

In numerical models for computing ELF electric and magnetic fields, the problem can be considered as quasistatic [9, 10]. Quasistatic fields vary slowly with time, and therefore, attenuation is equal to zero, whereas the phase shift of these fields can be neglected without a loss of accuracy. Hence, these fields may be computed separately.

In many papers, numerical algorithms for computing overhead power lines electric field are two-dimensional (2D) [11–13]. In these algorithms, overhead power line conductors are straight thin-wire horizontal lines parallel to a flat Earth's surface and parallel with each other. The number of line sources equals the number of overhead power line conductors and shield wires. Moreover, the influence of the sag is completely neglected or just roughly taken into account with the average height of the conductors.

In order to obtain more precise computation results of the electric field intensity distribution at any point under arbitrary complex configurations of the overhead power lines, 3D algorithms must be used. In 3D algorithms [14–18], the catenary form of the overhead power line conductors can be taken into account. In this paper, the catenary conductors are approximated by a set of straight thin-wire cylindrical segments.

In some papers [18–21], the authors have adopted the well-known fact that electric field is strongly perturbed by the presence of objects such as overhead power line towers, and therefore, have taken them into account. Thereat, different numerical methods, such as finite element method (FEM), charge simulation method (CSM) and boundary element method (BEM), were used. Solid metal objects, as well as the human body, are, in general, modelled with the surface charges, while their electric potential is equal to zero when they are grounded. Here, in order to determine the influence of the overhead power line towers to the electric field intensity distribution in their close vicinity, a similar approach is used. The basis of the developed method is the application of the finite element method to an integral equation formulation in the frequency domain. The real catenary form of the overhead power line phase conductors and shield wires is approximated by a set of straight thin-wire cylindrical segments of active and passive conductors whereas the towers are approximated using thin-wire cylindrical segments of passive conductors. Presented 3D quasistatic numerical model for computation of the electric field produced by overhead power lines is completely general; the number and length of overhead power line catenaries, heights and types of towers, as well as their mutual position, are arbitrary. In the chosen numerical example, the obtained results of the electric field intensity distribution are shown and compared with other computed and measured published results.

2. SEGMENTATION OF THE OVERHEAD POWER LINE CONDUCTORS

In general, many numerical algorithms for computing overhead power lines electric field are two-dimensional (2D). In these algorithms, overhead power line conductors satisfy a thin-wire approximation and are treated as infinite mutually parallel line sources positioned at a constant distance from a flat Earth's surface. The number of line sources equals the number of overhead power line phase conductors and shield wires.

Since the overhead power line conductors actually take the form of a catenary, these 2D algorithms are only a rough approximation, and therefore, precise computation of the electric field intensity distribution, especially when field points are in the vicinity of the overhead power lines, is not possible. Besides these analytical and numerical 2D models [11–13], some commercial software packages, which are widely used for computation of overhead power lines electric field, use the same simplified 2D algorithm. However, in a certain number of real cases, advanced 3D algorithms must be applied [14–18].

Overhead power line phase conductors and shield wires, which represent sources, are oriented along the x-axis in the global Cartesian coordinate system (x, y, z). The origin of the selected coordinate system is on the Earth's surface, which is represented by $z = 0$, and in the middle of the overhead power line section. Computation of the electric field is carried out in the y-z plane, perpendicular to the observed power line section.

Segmentation of the overhead power line conductors has to be done for each power line span separately. For the purpose of conductor segmentation applied to overhead power line span, the local coordinate system (u, z) is used. In the first step, observed conductor of overhead power line span is subdivided into two parts and then each of these parts is subdivided into m segments whose orthogonal projections are equal. The first part of the overhead power line conductor lies between the start point $T_b(-\ell/2, z_b)$ and the lowest point of the catenary curve $T_{\min}(u_{\min}, z_{\min})$, whereas the second part is located between $T_{\min}$ and the end point $T_e(\ell/2, z_e)$, as shown in Figure 1.

The input data for the conductor segmentation process are global coordinates of the points $T_b(x_b, y_b, z_b)$, $T_e(x_e, y_e, z_e)$ and height $z_{\min}$ of the lowest point $T_{\min}$. Prior to segmentation, it is necessary to compute the local coordinates of the start point of the overhead power line span conductor $T_b(-\ell/2, z_b)$, the end point $T_e(\ell/2, z_e)$ and $u_{\min}$. Overhead power line span conductors take the form of a catenary, which is described by cosine function in the local coordinate system (u, z):

$$z = z_{\min} \cdot \cosh \frac{u - u_{\min}}{a} \tag{1}$$

$$a = \frac{\dfrac{\ell}{2} - u_{\min}}{\cosh^{-1} \dfrac{z_e}{z_{\min}}} \tag{2}$$

where ℓ is length of the overhead power line span.
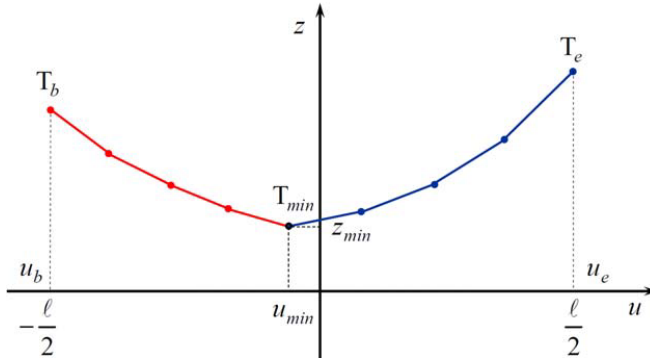
Figure 1. 3D model of the overhead power line span conductor.

It was found in [22] that approximation by ten straight segments per overhead power line span conductor can be taken as optimal from a geometrical point of view, but despite that, in electric field intensity computation, a larger number of segments per overhead power line span conductor are required.

3. SEGMENTATION OF THE OVERHEAD POWER LINE TOWERS

As well known [23], electric field is strongly perturbed in the vicinity of overhead power line towers, but despite that, many authors ignore their presence. Here, a computer program for detailed segmentation of typical steel lattice towers of various types has been developed. The towers are approximated using straight thin-wire cylindrical segments of passive conductors but moreover, they can be approximated using originally developed subparametric spatial 2D finite elements. In that case, four lateral surfaces represent four subparametric spatial 2D finite elements with an arbitrary number of nodes for a description of surface charge density distribution. Shape and mapping functions of these finite elements are developed and described in detail in [24].

Detailed segmentation of a one-circuit "Y" tower type is carried out only for tower base and tower body, while is neglected for tower top due to insignificant influence on computation results near the Earth's surface. In the first step of segmentation process, global coordinates of the tower base points, A_0, B_0, C_0 and D_0 (Figure 2), are determined from:

$$x_0 = x_s + \frac{\sqrt{d_1^2 + d_2^2}}{2} \cdot \cos\left(\alpha_0 + \beta\right) \tag{3}$$

$$y_0 = y_s + \frac{\sqrt{d_1^2 + d_2^2}}{2} \cdot \sin\left(\alpha_0 + \beta\right) \tag{4}$$

$$z_0 = 0 \tag{5}$$

$$\alpha_0 = \begin{cases} \pi + \tan^{-1}\dfrac{d_2}{d_1} & \text{for } A_0 \\[2mm] -\tan^{-1}\dfrac{d_2}{d_1} & \text{for } B_0 \\[2mm] \tan^{-1}\dfrac{d_2}{d_1} & \text{for } C_0 \\[2mm] \pi - \tan^{-1}\dfrac{d_2}{d_1} & \text{for } D_0 \end{cases} \tag{6}$$

where (x_s, y_s) are global coordinates of the center point S; d_1 and d_2 are length and width of the tower base; β is the swing angle of the tower relative to the coordinate system $(x, y, 0)$.

Thereafter, global coordinates of points A_n, B_n, C_n and D_n are determined, and main structural elements between these points are divided into $n - 1$ rods of the same length. It is necessary to define only a total number of segments in the developed computer program, and global coordinates of all points are obtained (Figure 3).
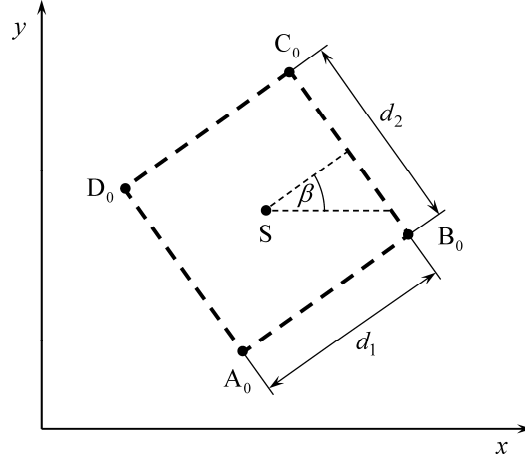
Figure 2. Ground plan of the overhead power line tower base.
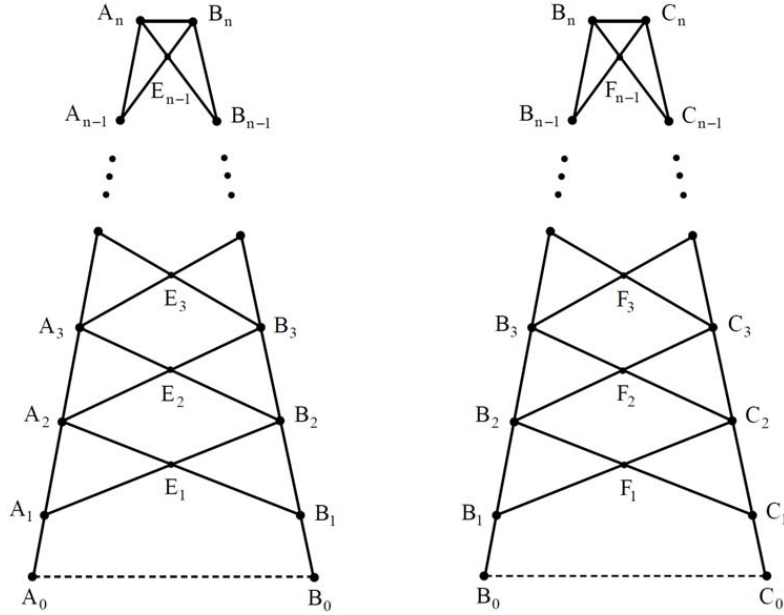
Figure 3. Segmentation of the overhead power line tower.

4. COMPUTATION OF THE CHARGE DENSITY DISTRIBUTION

Components of the quasistatic electromagnetic model for computation of ELF overhead power lines electric field are straight thin-wire cylindrical segments of active and passive conductors.

In this paper, a two-layer medium is observed, in which the first layer is air, characterised by vacuum permittivity ε_0 and permeability μ_0, while the second layer is homogeneous earth, characterised by relative permittivity ε_r, permeability μ_0 and electrical conductivity κ.

Using the well-known Galerkin-Bubnov method, a symmetric system of linear equations for computation of charge density distribution can be obtained using the following expression:

$$\int_{\Gamma_i} (\bar{\varphi} - \bar{\Phi}_i^s) \cdot d\ell_i = 0; \quad i = 1, \dots, NS \tag{7}$$

where $\bar{\varphi}$ is the phasor of the computed value of the scalar electric potential, $\bar{\Phi}_i^s$ the phasor of the prescribed potential of the i-th cylindrical conductor segment assumed to be constant, Γ_i the integration

path positioned along the i-th cylindrical conductor segment axis, and NS the total number of cylindrical conductor segments.

From Eq. (7), the following system of linear equations, written in matrix form, can be obtained:

$$\left[\overline{PSS}\right] \cdot \{\bar{\lambda}\} = \{\Psi^s\} \tag{8}$$

where $\left[\overline{PSS}\right]$ is the matrix of the self and mutual coefficients joined to the cylindrical conductor segments, $\{\bar{\lambda}\}$ the cylindrical conductor segments linear charge density vector, and vector $\{\Psi^s\}$ can be described using the following expression:

$$\{\Psi^s\} = \left\{ \begin{array}{c} \bar{\Phi}_1^s \cdot \ell_1 \\ \vdots \\ \bar{\Phi}_{NS}^s \cdot \ell_{NS} \end{array} \right\} \tag{9}$$

5. SCALAR ELECTRIC AND VECTOR MAGNETIC POTENTIALS

Cylindrical conductor segment linear charge density is approximated by a constant, hence the scalar electric potential distribution at the arbitrary field point $T(x, y, z)$ in the air of the observed two-layer medium can be written as:

$$\bar{\varphi} = \sum_{i=1}^{NS} \frac{\bar{\lambda}_i}{4 \cdot \pi \cdot \varepsilon_0} \cdot \left(\int_{\Gamma_i} \frac{d\ell_i}{R_i} + \bar{k}_r \cdot \int_{\Gamma_{i^s}} \frac{d\ell_i}{R_{i^s}} \right) \tag{10}$$

where $\bar{\lambda}_i$ is the phasor of the i-th cylindrical conductor segment linear charge density, Γ_{i^s} the integration path positioned along the axis of the i-th cylindrical conductor segment image, R_i the distance between the field point and a source point, R_{i^s} the distance between the field point and a source image point, and $\bar{k}_r$ the reflection coefficient, which can be approximated to high accuracy by $\bar{k}_r = -1$ as a consequence of assumption that the Earth's conductivity is infinite [25] (Figure 4).
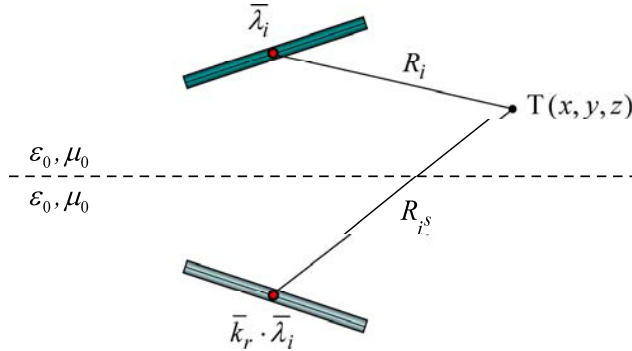
Figure 4. Cylindrical conductor segment and its image.

The boundary conditions are potentials of cylindrical conductor segments, zero potential of the Earth's surface and zero potential at infinity. For each straight thin-wire cylindrical conductor segment, the longitudinal current and unit vector are directed from the start point to the end point of the segment. Since the permeability of the entire medium has the same value, the distribution of the vector magnetic potential due to longitudinal currents of the overhead power line cylindrical conductor segments is described by the following expression, valid for homogeneous and unbounded media:

$$\vec{\underline{A}} = \frac{\mu_0}{4 \cdot \pi} \cdot \sum_{i=1}^{NS} \vec{s}_{0\,i} \cdot \bar{I}_i \cdot \int_{\Gamma_i} \frac{d\ell}{R_i} \tag{11}$$

where $\vec{\underline{A}}$ is the phasor of the vector magnetic potential, $\bar{I}_i$ the phasor of the i-th conductor segment current, and $\vec{s}_{0\,i}$ the unit vector of the i-th cylindrical conductor segment.

6. COMPUTATION OF THE ELECTRIC FIELD INTENSITY

The phasor of the electric field intensity at the arbitrary field point $T\,(x, y, z)$ in the air can be computed from Eqs. (10) and (11) using the following expression:

$$\vec{\underline{E}} = \left\{ \bar{E}_x, \bar{E}_y, \bar{E}_z \right\} = -\nabla \bar{\varphi} - j \cdot \omega \cdot \vec{\underline{A}} \tag{12}$$

where $\bar{E}_x$, $\bar{E}_y$ and $\bar{E}_z$ are x-, y- and z-axis phasor components of the electric field intensity, which are obtained by contributions of all NS cylindrical conductor segments using the superposition technique.

It can be seen from Eq. (12) that quasistatic electric field in the air includes the divergent component and rotational component of the electric field, although the latter, which is taken into account here, can be neglected without loss of accuracy.

7. NUMERICAL EXAMPLE

A real catenary form of the overhead power line conductors is taken into account, as well as towers, to illustrate the effect of conductor sag and proximity effect of towers on the electric field intensity distribution.

On the basis of the presented theory, a FORTRAN program PFEMF (Power Frequency Electro Magnetic Field) for computation of the rms values of the electric field intensity distribution is developed.

For this purpose, two spans between three identical towers of a typical $400\,\mathrm{kV}$ overhead power line (Figure 5), each carrying three phases (L1, L2 and L3) with two conductors in the bundle per phase and two shield wires (SW1 and SW2) in the horizontal disposition, are observed. Detailed electrical and geometrical input data for conductors and tower dimensions are given in [26]. It is assumed that the maximum allowed conductor current flows through the phase conductors, while phase voltage value was also symmetrical and equal to $241.8\,\mathrm{kV}$. The length of the overhead power line span is equal to $\ell = 300\,\mathrm{m}$, while lowest points of all conductors have unequal heights. Each span is approximated by 60 straight thin-wire cylindrical segments of active and passive conductors. Two different cases are observed:
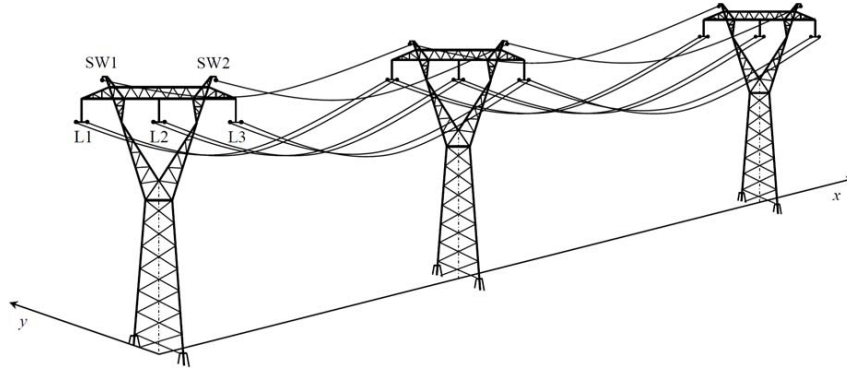
Figure 5. $400\,\mathrm{kV}$ overhead power line.

Case 1 — only phase conductors and shield wires (16 catenaries, each approximated using 60 thin-wire cylindrical segments) are taken into account, whereas towers are neglected;
Case 2 — catenaries from Case 1 are taken into account, but also a central tower is approximated using 68 thin-wire cylindrical segments of passive conductors.

Computation of the electric field intensity distribution is carried out at $1\,\mathrm{m}$ above the Earth's surface in the close vicinity of a central tower along the x- and y-axes. In both directions, the start point is $0.2\,\mathrm{m}$ away from the base of the observed tower. Hence, start points along the observed longitudinal and perpendicular axes have coordinates $x = 2.0\,\mathrm{m}$ and $y = 2.5\,\mathrm{m}$, respectively. Computation is conducted at 1000 points along these axes, to the end points with coordinates $x = 22.0\,\mathrm{m}$ and $y = 22.5\,\mathrm{m}$, respectively.

Figures 6–9 present computed effective values of the electric field intensity components and total effective values of the electric field intensity distribution along observed x- and y-axes for the aforementioned cases.
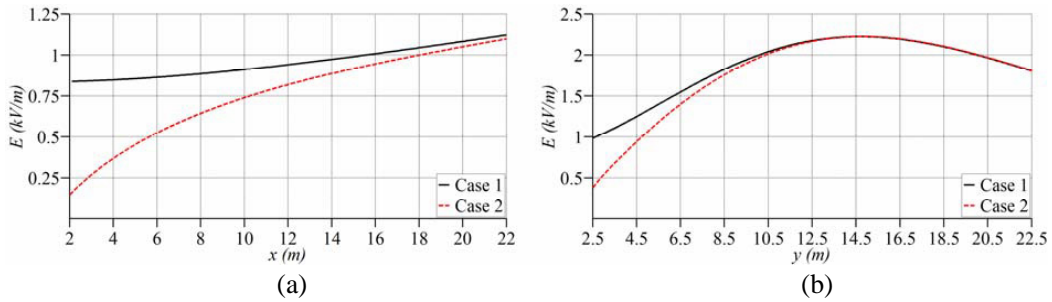
Figure 6. Distribution of the total electric field intensity along: (a) x-axis, (b) y-axis.
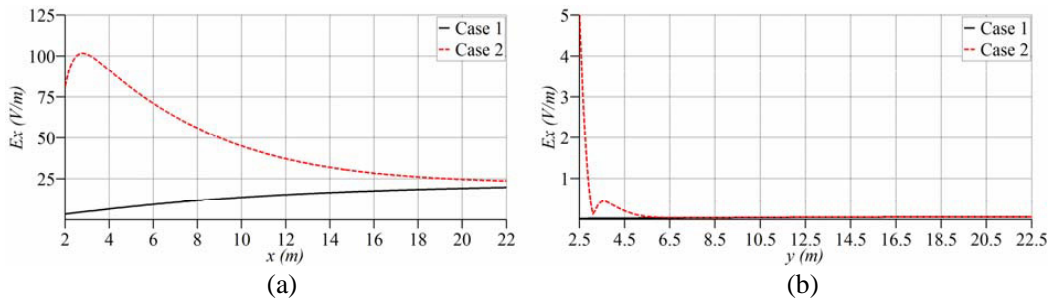
Figure 7. Electric field intensity x-component along: (a) x-axis, (b) y-axis.
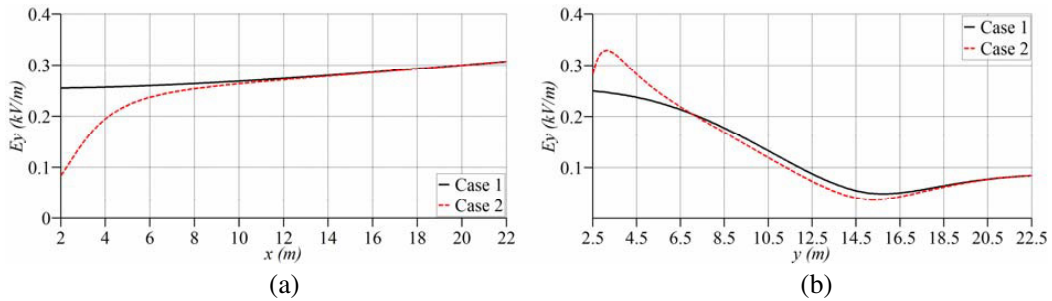
Figure 8. Electric field intensity y-component along: (a) x-axis, (b) y-axis.
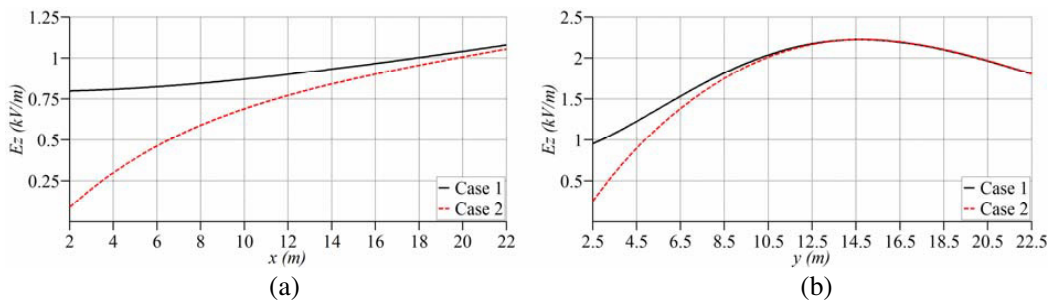
Figure 9. Electric field intensity z-component along: (a) x-axis, (b) y-axis.

As can be clearly seen from Figures 6–9, overhead power line towers distort the electric field in their close vicinity and reduce its magnitude. Therefore, they cannot be ignored in the computation of the nearby electric field intensity.

The influence of the towers can be seen from spatial distribution of the total electric field intensity shown in Figures 10 and 11, with and without the presence of the towers. In these figures, two towers at positions with coordinates $x = 0\,\mathrm{m}$ and $x = 300\,\mathrm{m}$ are approximated using thin-wire cylindrical segments of passive conductors. These spatial distributions of the total electric field intensity with and without the presence of the towers are also given in the x-y plane in Figures 12 and 13. Different magnitudes of the electric field intensity at towers positions can be easily seen.
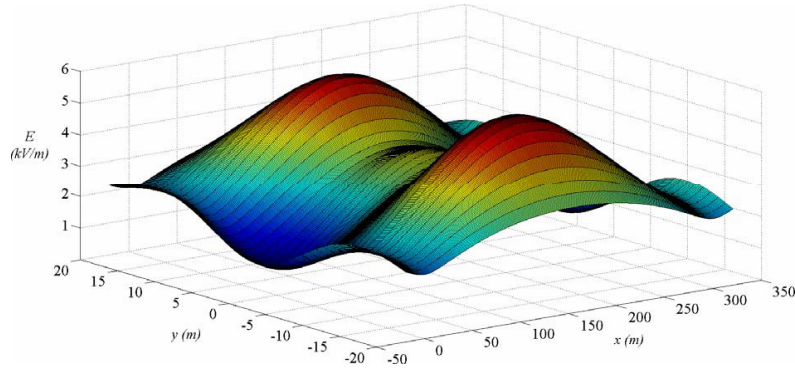
Figure 10. Spatial distribution of the electric field intensity without the presence of the towers.
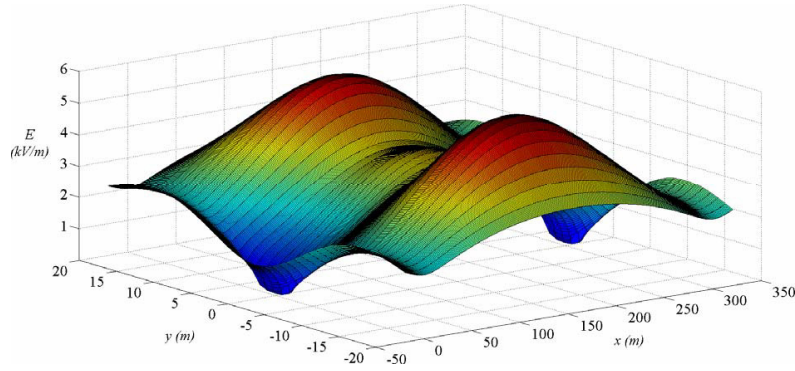
Figure 11. Spatial distribution of the electric field intensity with the presence of the towers.
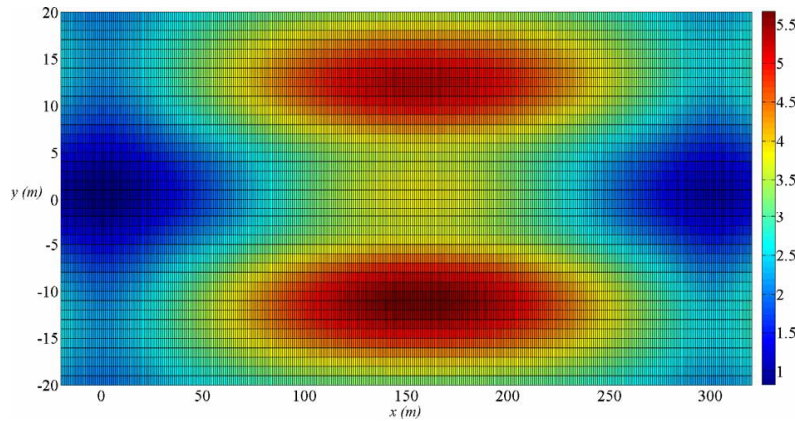
Figure 12. Electric field intensity in the x-y plane without the presence of the towers.
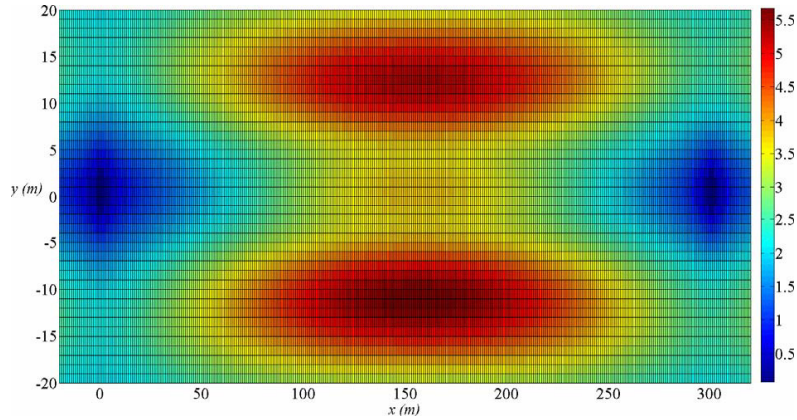
Figure 13. Electric field intensity in the x-y plane with the presence of the towers.

In order to verify the accuracy of the presented model, the obtained results were compared with those of a one-circuit "Y" tower type of similar input data and geometry, analysed in [20]. Figures 14–17 show the effective values of the total electric field intensity and electric field intensity components at 1 m above the Earth's surface along x- and y-coordinate axes, with and without the presence of the tower. A very good concordance can be seen with relative figures provided in [20].
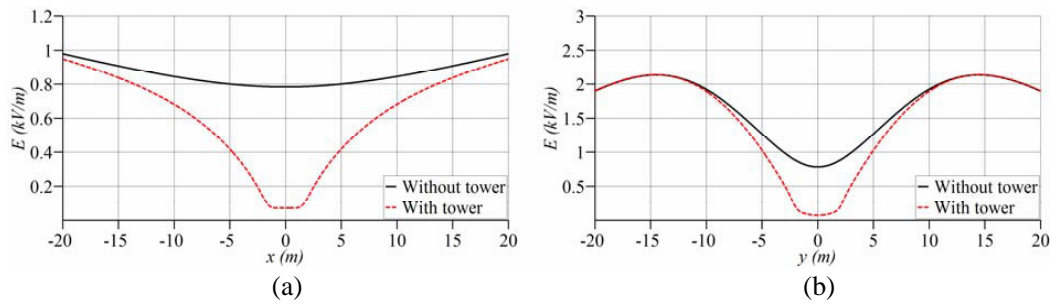
Figure 14. Total electric field intensity with and without the tower along: (a) x-axis, (b) y-axis.
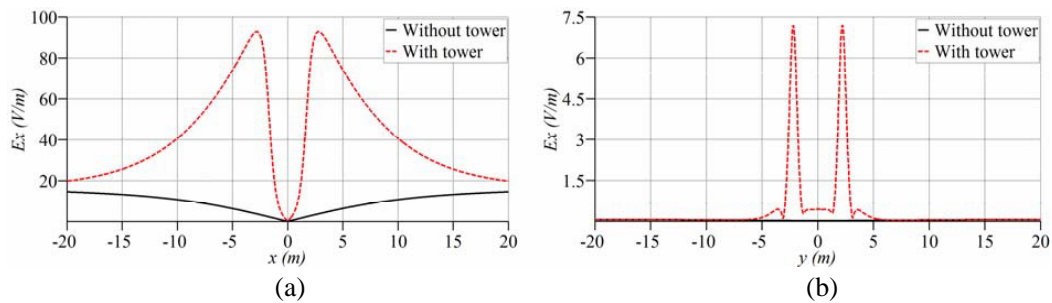
Figure 15. Electric field intensity x-component with and without the tower along: (a) x-axis, (b) y-axis.

The effect of conductor sag can be obtained under the midspan, where the influence of the towers can be ignored and due to the minimum conductor heights, a maximum value of the electric field may be expected. The obtained results were compared with the measured and computed ones [17, 28] (Figure 18) and once again, a very good agreement is achieved which validates the accuracy of the presented model.
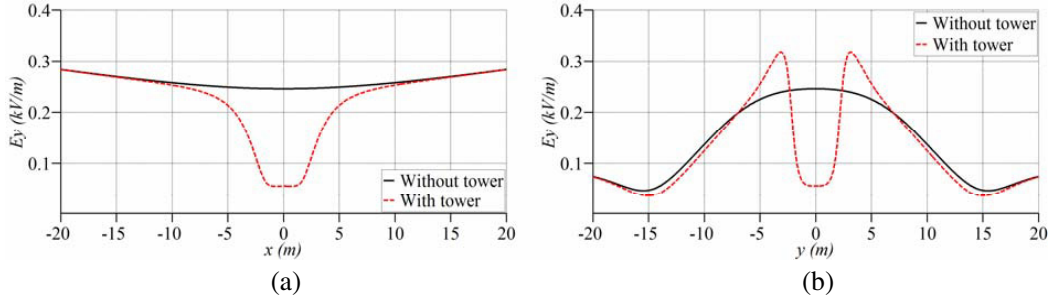
Figure 16. Electric field intensity y-component with and without the tower along: (a) x-axis, (b) y-axis.
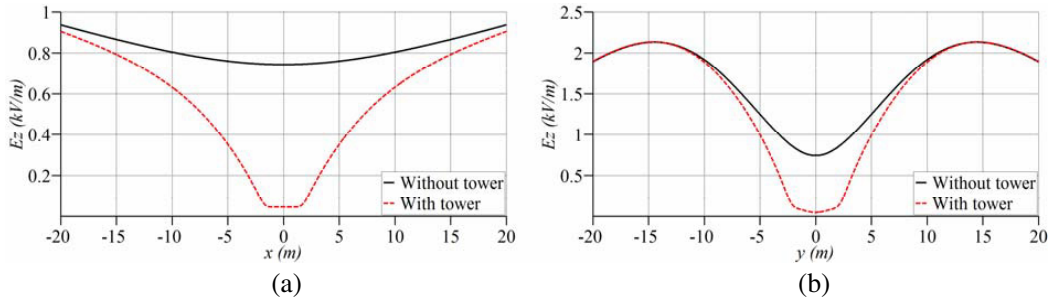
Figure 17. Electric field intensity z-component with and without the tower along: (a) x-axis, (b) y-axis.
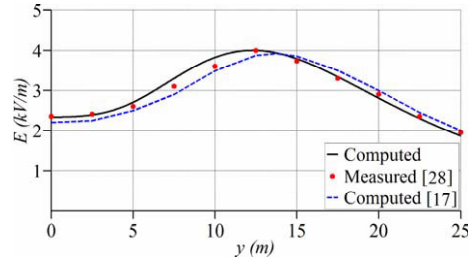
Figure 18. Comparison of obtained results with results available in the literature.

8. CONCLUSIONS

In this paper, a 3D quasistatic numerical method for computation of the electric field produced by overhead power lines is presented. The basis of the developed algorithm is the application of the finite element method to an integral equation formulation in the frequency domain. The real catenary form of the overhead power line phase conductors and shield wires is approximated by a set of straight thin-wire cylindrical segments of active and passive conductors. The segmentation algorithm is completely general and requires minimum geometrical input data and number of segments. The electrical input data are conductors phase voltages and longitudinal currents, which are known and can be unsymmetrical. Moreover, the towers of the overhead power lines are approximated using thin-wire cylindrical segments of passive conductors. The towers are taken into account as a grounded object with zero potential. A computer program for detailed segmentation of typical steel lattice towers of various types is developed. The segmentation process is simplified in such a way that global coordinates of all points can be easily obtained after the number of cylindrical segments for geometrical approximation has been defined. All of these active and passive segments contribute to the electric field intensity distribution. In the numerical example, electric field intensity distribution in the vicinity of the towers and under the midspan is shown.

The obtained results are compared with other published results available in the literature, and a very good concordance can be seen. In order to obtain more precise results of the electric field intensity distribution, a real catenary form of the overhead power line conductors, as well as towers, must be taken into account.

REFERENCES

1. Stuchly, M. A. and T. W. Dawson, "Interaction of low-frequency electric and magnetic fields with the human body," *Proceedings of the IEEE*, Vol. 88, No. 5, 643–664, 2000.

2. Siauve, J. N., R. Scorretti, N. Burais, L. Nicolas, and A. Nicolas, "Electromagnetic fields and human body: A new challenge for the electromagnetic field computation," *The International Journal for Computation and Mathematics in Electrical and Electronic Engineering*, Vol. 22, 457–469, 2003.

3. King, R. W. P., "A review of analytically determined electric fields and currents induced in the human body when exposed to 50–60-Hz electromagnetic fields," *IEEE Transactions on Antennas and Propagation*, Vol. 52, No. 5, 1186–1192, 2004.

4. Din, E. S. T. E., H. Anis, and M. Abouelsaad, "A probabilistic approach to exposure assessment of power lines electric field," *IEEE Transactions on Power Delivery*, Vol. 20, No. 2, 887–893, 2005.

5. Teepen, J. C. and J. A. van Dijck, "Impact of high electromagnetic field levels on childhood leukemia incidence," *International Journal of Cancer*, Vol. 131, No. 4, 769–778, 2012.

6. IARC, "Non-ionizing radiation, Part 1: Static and extremely low-frequency (ELF) electric and magnetic fields," *IARC Monographs on the Evaluation of Carcinogenic Risks to Humans*, Vol. 80, 1–395, 2002.

7. WHO, "Extremely low frequency fields, Environmental Health Criteria Monograph No. 238," WHO Press, Geneva, Switzerland, 2007.

8. International Commission on Non-Ionizing Radiation Protection, "Guidelines for limiting exposure to time-varying electric and magnetic fields (1 Hz to 100 kHz)," *Health Physics*, Vol. 99, No. 6, 818–836, 2010.

9. Olsen, R. G. and P. S. Wong, "Characteristics of low frequency electric and magnetic fields in the vicinity of electric power lines," *IEEE Transactions on Power Delivery*, Vol. 7, No. 4, 2046–2055, 1992.

10. Fitzpatrick, R., *Maxwell's Equations and the Principles of Electromagnetism*, Infinity Science Press LLC, Hingham, 2008.

11. Tzinevrakis, A. E., D. K. Tsanakas, and E. I. Mimos, "Analytical calculation of the electric field produced by single-circuit power lines," *IEEE Transactions on Power Delivery*, Vol. 23, No. 3, 1495–1505, 2008.

12. Vujević, S., D. Lovrić, and P. Sarajčev, "Comparison of 2D algorithms for the computation of power line electric and magnetic fields," *European Transactions on Electrical Power*, Vol. 21, No. 1, 505–521, 2011.

13. Nicolaou, C. P., A. P. Papadakis, P. A. Razis, G. A. Kyriacou, and J. N. Sahalos, "Measurements and predictions of electric and magnetic fields from power lines," *Electric Power Systems Research*, Vol. 81, No. 5, 1107–1116, 2011.

14. Amiri, R., H. Hadi, and M. Marich, "The influence of sag in the electric field calculation around high voltage overhead transmission lines," *IEEE Conference of Electrical Insulation and Dielectric Phenomena*, 206–209, Kansas City, MO, 2006.

15. Yang, Y., J. Lu, and Y. Lei, "A calculation method for the electric field under double-circuit HVDC transmission lines," *IEEE Transactions on Power Delivery*, Vol. 23, No. 4, 1736–1742, 2008.

16. Salari, J. C., A. Mpalantinos, and J. I. Silva, "Comparative analysis of 2- and 3-D methods for computing electric and magnetic fields generated by overhead transmission lines," *IEEE Transactions on Power Delivery*, Vol. 24, No. 1, 338–344, 2009.

17. El Dein, A. Z., "Parameters affecting the charge distribution along overhead transmission lines' conductors and their resulting electric field," *Electric Power Systems Research*, Vol. 108, 198–210, 2014.

18. Modrić, T. and S. Vujević, "Computation of the electric field in the vicinity of overhead power line towers," *Electric Power Systems Research*, Vol. 135, 68–76, 2016.

19. Krajewski, W., "Numerical assessment of electromagnetic exposure during live-line works on high-voltage objects," *IET Science, Measurement and Technology*, Vol. 3, No. 1, 27–38, 2009.

20. Zemljaric, B., "Calculation of the connected magnetic and electric fields around an overhead-line tower for an estimation of their influence on maintenance personnel," *IEEE Transactions on Power Delivery*, Vol. 26, No. 1, 467–474, 2011.

21. El Dein, A. Z., "Calculation of the electric field around the tower of the overhead transmission lines," *IEEE Transactions on Power Delivery*, Vol. 29, No. 2, 899–907, 2014.

22. Modrić, T., S. Vujević, and T. Majić, "Geometrical approximation of the overhead power line conductors," *International Review on Modelling and Simulations*, Vol. 7, No. 1, 76–82, 2014.

23. "IEEE Standard procedures for measurement of power frequency electric and magnetic fields from AC power lines," The Institute of Electrical and Electronics Engineers, Inc., ANSI/IEEE Std 644-1987, New York, 1994.

24. Modrić, T., S. Vujević, and D. Lovrić, "A surface charge simulation method based on advanced numerical integration," *Advances in Engineering Software*, Vol. 86, 20–28, 2015.

25. Stratton, J. A., *Electromagnetic Theory*, McGraw-Hill Book Company, New York, 1941.

26. Modrić, T., S. Vujević, and D. Lovrić, "3D computation of the power lines magnetic field," *Progress In Electromagnetics Research M*, Vol. 41, 1–9, 2015.

27. Mujezinović, A., A. Čarsimamović, S. Čarsimamović, A. Muharemović, and I. Turković, "Electric field calculation around of overhead transmission lines in Bosnia and Herzegovina," *Proceedings of the 2014 International Symposium on Electromagnetic Compatibility (EMC Europe 2014)*, 1001–1006, Gothenburg, Sweden, 2014.

28. Carsimamovic, S., Z. Bajramovic, M. Rascic, M. Veledar, E. Aganovic, and A. Carsimamovic, "Experimental results of ELF electric and magnetic fields of electric power systems in Bosnia and Herzegovina," *IEEE International Conference on Computer as a Tool (EUROCON)*, Lisbon, Portugal, 2011.